Reovirus type-2–triggered autoimmune cholangitis in extrahepatic bile ducts of weanling DBA/1J mice

Tomomi Nakashima[1], Toshiharu Hayashi[1], Saki Tomoeda[1], Midori Yoshino[1] and Takuya Mizuno[2]

BACKGROUND: Reovirus is a proposed cause of infantile biliary atresia. However, mechanistic insight regarding Reo-2 as a potential cholangiotropic virus is lacking. Furthermore, it is unknown whether Reo-2 infection can induce autoimmune-mediated bile duct injury.

METHODS: Lesions of bile ducts in newborn DBA/1J mice infected with Reo-2 were analyzed immunopathologically.

RESULTS: Damage to biliary epithelia occurs after Reo-2 infection. In addition, nonsuppurative cholangitis with fibrosis in extrahepatic (especially septal) bile ducts developed following complete viral clearance from the liver. At the inflamed ducts, major histocompatibility complex class I expressing$^{(+)}$ and FAS$^+$ cholangiocytes were associated with FAS ligand$^+$ lymphocytes and tumor necrosis factor-α^+ mononuclear cells (macrophages and lymphocytes). These cholangiocytes were apoptotic and necrotic. Moreover, affected ducts were infiltrated by CD3$^+$, CD4$^+$, CD8$^+$, IFN-γ^+, and FAS$^+$ lymphocytes. Analysis of blood from Reo-2–infected mice revealed that they developed anti-cholangiocyte cytoplasm antibodies and had high serum IFN-γ concentration. Notably, there was no increase in Foxp3$^+$ lymphocytes at inflamed ducts, lymph nodes, and thymi.

CONCLUSION: Reo-2 infection induced T-helper cell type 1–dependent injury to bile ducts in weanling mice. The lesions observed in mice may be analogous to those associated with human infantile biliary atresia, which are caused by an autoimmune-mediated process.

Biliary atresia is the most common cause of neonatal cholestasis and is characterized by progressive sclerosing cholangitis of the extrahepatic biliary tree (1,2). Although the etiology of biliary atresia is not completely understood, several factors have been proposed (1–3). These include viral infection of the primary perinatal hepatobiliary epithelium and autoimmune-mediated bile duct injury (1). Two *Reoviridae* virusues, group C rotavirus and reovirus type (Reo)-3, have been implicated as causative agents of biliary atresia (2). It has been reported that, the anatomical and inflammatory profiles associated with rotavirus-induced biliary atresia in mice share striking similarities with those of human biliary atresia (3,4).

Reovirus is a ubiquitous, nonenveloped, cytoplasmically replicating virus isolated from a wide variety of mammalian species, including humans (5,6). Reovirus consists of three serotypes and is considered an "orphan virus" because no definitive links to disease have been established. However, several reports suggest that reovirus may be associated with diarrheal illnesses, upper respiratory infections, and hepatobiliary diseases, including biliary atresia and rare infections of the central nervous system (5,7). For instance, animals infected either naturally or experimentally with Reo-3 develop various diseases (5). In addition, Reo-3 replicates in the cytoplasm of extrahepatic biliary epithelia and causes acute, transient, or segmental cholangitis in weanling mice (8–10). High levels of Reo-3 were found in the serum of a 6-week-old female rhesus monkey with jaundice and conjugated hyperbilirubinemia (11). Reo-3 antigens and virus-like particles were found in the bile duct of a patient with biliary atresia (12) and in patients with extrahepatic biliary atresia or choledochal cysts (13).

We previously reported that Reo-2 infection within 24 h after birth in weanling DBA/1J mice induces transient helper T (Th)–1 dominant autoimmune insulitis with impaired glucose tolerance (6). In addition, the autoimmune disease susceptibility locus (first chromosome *VAS1* gene) in DBA/1J mice is involved with the development of insulitis (14). Thymic atrophy in conjunction with the production of autoantibodies suggests that autoimmune responses may be formed in Reo-2–infected weanling mice (6)). Thus, we propose that cholangiotropic Reo-2 infection and subsequent autoimmune-induced bile duct injury may potentiate the development of infantile biliary atresia. To address this, we studied the mechanism of Reo-2 infection and its effects on immune-mediated injury to extrahepatic bile ducts in a mouse model.

RESULTS

Virus Replication in the Liver and Serum Alkaline Phosphatase Levels

Isolation of virus at 3 and 5 d postinfection (dpi) yielded 2.5×10^2 and 1.25×10^3 plaque-forming units per gram, respectively. Virus was undetectable at 7–13 dpi (**Figure 1a**). Serum alkaline phosphatase levels increased significantly at 7, 13, and 21 dpi in infected mice, when compared with uninfected controls (**Figure 1b**; $P < 0.05$).

[1]Laboratory of Veterinary Pathology, Joint Faculty of Veterinary Medicine, Yamaguchi University, Yamaguchi, Japan; [2]Veterinary Internal Medicine, Joint Faculty of Veterinary Medicine, Yamaguchi University, Yamaguchi, Japan. Correspondence: Toshiharu Hayashi (hayasi@yamaguchi-u.ac.jp)

Received 6 February 2013; accepted 23 May 2013; advance online publication 22 January 2014. doi:10.1038/pr.2013.170

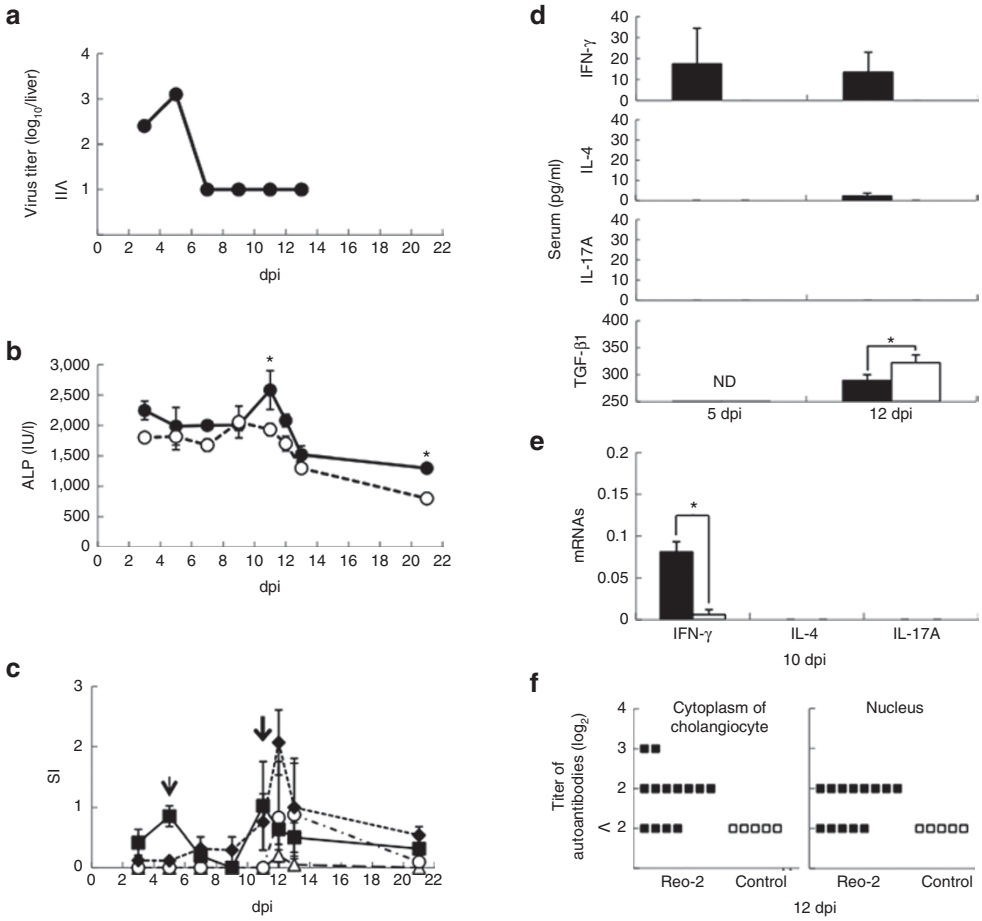

Figure 1. Virus titer, alkaline phosphatase (ALP), score index (SI) values, and mRNA expression for cytokines and production of autoantibodies. (**a**) Virus titer in livers (black circles: Reo-2 infected); (**b**) ALP values in sera (black circles: Reo-2 infected and white circles: control); (**c**) SI (black squares: bile ductal damage; black rhombuses: inflammation; white circles: proliferation of biliary epithelium; white triangles: fibrosis in extrahepatic septal ducts; and thin and bold arrows: peaks of epithelial destruction at 5 and 11 dpi, respectively); values in (**d**) serum or (**e**) mRNA expression from splenocytes of IFN-γ, IL-4, TGF-β1, and/or IL-17A; and (**f**) titer of autoantibodies against cytoplasm of cholangiocytes (ductal epithelium) in liver and nucleus of hepatocytes (black squares: Reo-2 infected and white squares: control). Data are presented as mean ± SEM except for **c** (mean ± SD). *$P < 0.05$ compared with the control. dpi, days postinfection; ND, not done.

Extrahepatic Bile Duct Lesion (Score Index)

Upon Reo-2 infection, inflammation developed in the extrahepatic septal bile ducts (Figure 1c). We observed two events of epithelial destruction at 5 and 11 dpi. Infiltration of mononuclear cells and proliferation of epithelia began at 7 dpi and peaked at 12 dpi. Those lesions persisted to 21 dpi but inflammation reduced.

Production of IFN-γ and TGF-β1 in Serum and mRNA Expression of IFN-γ, IL-4, and IL-17A in Splenocytes

At 5 and 12 dpi, the infected mice had significantly increased serum IFN-γ values and no or a little production of IL-4 and IL-17A, whereas there was no production of any of these three cytokines in the control mice (Figure 1d). TGF-β1 levels decreased in the infected mice compared with control mice. Increased IFN-γ mRNA expression was detected in splenocytes in the infected mice at 10 dpi (Figure 1e). There was no mRNA expression of IL-4 and IL-17 in both groups (Figure 1e).

Production of Autoantibodies Against Cholangiocytes

Autoantibodies against cholangiocyte-specific nuclear and cytoplasmic factors were detected in sera of the infected mice. Specifically, autoantibodies were detected at 12 dpi (Figure 1f). The titer of cholangiocyte-specific anticytoplasmic antibodies was higher than that of antinuclear antibodies.

Nonsuppurative Inflammation After Reo-2 Clearance in Intra- and Extrahepatic Bile Ducts

Extramedullary hematopoiesis containing erythrocytes and leukocytes was observed in the intrahepatic portal and parenchymal tissue of infected and control mice at 3–12 dpi. Although limited extramedullary hematopoiesis was observed in extrahepatic bile ducts, it decreased gradually from 13 to 21 dpi. Minor lesions formed in the interlobular ducts and large bile ducts. These lesions were less severe than those of the extrahepatic septal ducts. In addition, several focal necroses formed in the parenchyma at 3 and 5 dpi but were no longer detectable after 5 dpi.

At 3 and 5 dpi, some cholangiocytes and inflammatory cells were necrotic and apoptotic (data not shown). They were also structurally irregular and were located in slightly damaged ducts (Figure 2a). Notably, viral antigens were detected in these cholangiocytes and hepatocytes (Figure 2b).

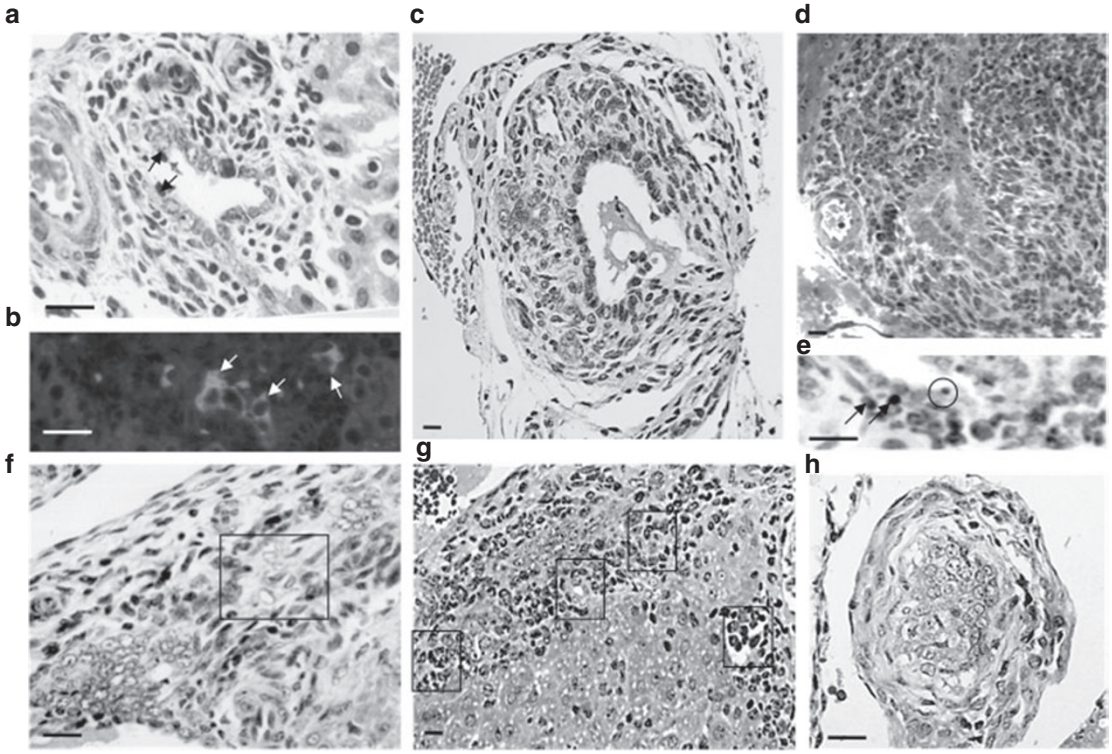

Figure 2. Histology of the cholangiocytes in the septal bile duct and bile ductule. (**a**) Shrunken cholangiocytes with pyknotic nuclei (arrows: suggestive of apoptosis), degeneration of epithelial cells with few inflammatory cells, and extramedullary hematopoiesis (EMH) are visible. (**b**) Viral antigens in cholangiocytes (arrows) are detected at 5 dpi. (**c**) Irregular shaped ducts with partial destruction of cholangiocytes and infiltrating mononuclear cells (lymphocytes and macrophages) around bile ducts at 7 dpi are shown. (**d**) The cholangiocytes show swelling and disordered polarity induced by severe infiltration of mononuclear cells, leading to stenosis and destruction of bile ducts at 12 dpi. (**e**) In these lesions, apoptosis of cholangiocytes (arrows) and some infiltrating lymphocytes (circle) can be seen. (**f**) Moreover, ductopenia due to fibrosis (rectangle in **f** indicates the process of loss of bile ducts), including proliferation of bile ductules (rectangles in **g**) are visible. (**h**) Obstruction of bile ducts with proliferated and degenerated cholangiocytes by slight fibrosis (onion skin appearance) is seen at 21 dpi. **a**, **c**, **f**, **g**, **h**: HE; **b**: IF; **d**: TB (semi-thin section); and **e**: TUNEL. **a**, **b**, **e**: original magnification ×950; **c**, **d**, **g**: original magnification ×350; and **f**, **h**: original magnification ×750. Bar = 50 μm. dpi, days postinfection; HE, hematoxylin and eosin; IF, immunofluorescence; TB, toluidine blue.

Accordingly, slight-to-mild infiltration of mononuclear cells was detected at 7–9 dpi (Figure 2c). At this stage, viral antigens were no longer detectable in the extrahepatic bile ducts or in the hepatic lesions. At 11–13 dpi, slight-to-severe infiltration of mononuclear cells and damage to the epithelia (Figure 2d) were observed. This was followed by the formation of necrotic and apoptotic cells (Figure 2e). There were slight-to-severe stenosis, bile ductal loss, or ductopenia with mild fibrosis (Figure 2f). At this phase, proliferation of bile ductules was recognized (Figure 2g). At 21 dpi, bile duct obstruction with a slight fibrosis around ducts was seen (Figure 2h).

Ultrastructure Changes of Extrahepatic Bile Ducts

At 12 dpi, no virus particles were observed in septal bile ducts. Bile ducts were relatively intact in case of lacking of inflammatory cell infiltration into epithelial layers despite irregular structure and damage of basement membranes (Figure 3a). Epithelia were infiltrated with macrophages and small- to mid-sized lymphocytes, containing little cytoplasm and few organelles (Figure 3b,c). Thereafter, those leukocytes had fully infiltrated the epithelium and were docked on cholangiocytes (Figure 3d). At this stage, cholangiocytes were highly apoptotic and necrotic (Figure 3e). Moreover, macrophage-engulfed apoptotic lymphocytes and abnormal basement membrane structure (e.g., discontinuous, irregular, or lytic) were routinely detected. In addition, dendritic cells having fewer phagocytic vacuoles, lysosomes, phagosomes, and phagolysosomes were recognized in the inflamed epithelial layers.

Detection of Autoantigens and Protein Expression in Cholangiocytes and Infiltrated Mononuclear Cells

Sera from the infected mice recognized cytoplasm of cholangiocytes but not that of hepatocytes, pancreatic duct cells, and acinar cells (Figure 4a). Moreover, sera from the infected mice recognized nuclear factors of cholangiocytes, hepatocytes, acinar cells, and pancreatic ductal cells (Figure 4b). At the inflamed site, major histocompatibility complex class I antigens were strongly expressed on cholangiocytes (Figure 4c) and weakly expressed on mononuclear cells. Infiltrated mononuclear cells consisted of macrophages (Figure 4d) and lymphocytes that were $CD3^+$ (Figure 4e), IFN-γ^+ (Figure 4f), $CD4^+$, or $CD8^+$. FAS^+ cholangiocytes were strongly associated with $FASL^+$ infiltrating mononuclear cells (Figure 4g). Moreover, weak expression of FAS^+ lymphocytes and moderate expression of $FASL^+$ cholangiocytes were observed (Figure 4h). Moreover, TNF-α^+ mononuclear cells were strongly associated with ducts. The

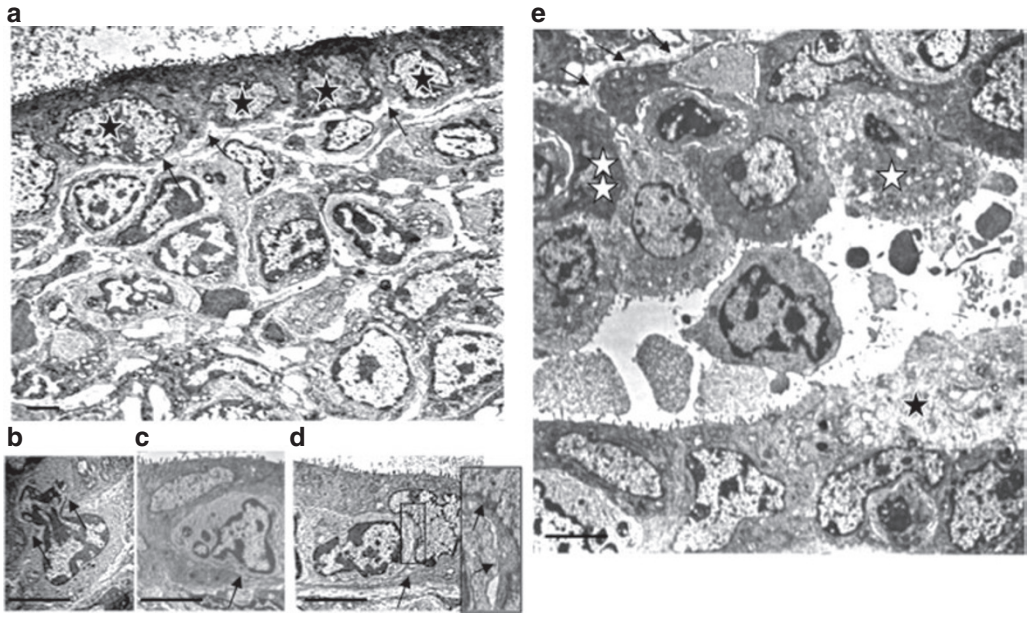

Figure 3. Ultrastructure of the cholangiocytes in septal bile ducts. (**a**) Cholangiocytes (black stars) are relatively intact due to a lack of lymphocyte and macrophage invasion. (**b**) Intraepithelial migration and (**c**) infiltration of lymphocytes are visible. (**d**) Attachment of lymphocytes to cholangiocytes and intrusion of cytoplasmic process of lymphocytes into cholangiocytes (arrows in inset: enlargement of rectangle in **d**) lead to (**e**) degeneration (black star) and apoptosis (white star) of cholangiocytes. Among them, dendritic cells (double white stars) can be seen. Long arrows in **a**–**d** indicate basement membranes. **a**: ×4,000; **b**–**e**: ×7,500; and inset in **d**: ×14,000 (original magnification). 12 d post infection. Bar =5 μm.

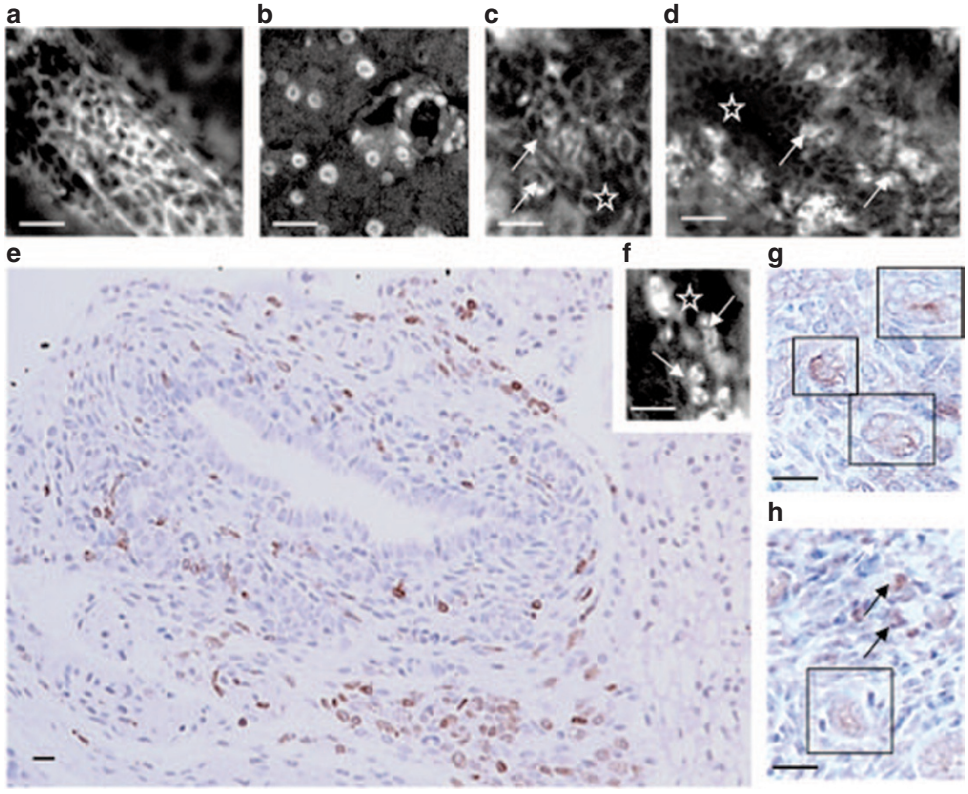

Figure 4. Reactivity of autoantibodies and immunohistochemistry. (**a**,**b**) Autoantibodies to normal cells and (**c**–**h**) expression of proteins in cholangiocytes and infiltrated cells. (**a**) High titers of sera from infected mice, which do not react with nucleus at this dilution, recognized cytoplasmic antigens of cholangiocytes but not of hepatocytes in uninfected mice. (**b**) Low titers of sera from infected mice recognized nuclei of pancreatic ducts and acini, but not their cytoplasm, of uninfected mice. Intense major histocompatibility complex class I expression on destructed cholangiocytes (arrows in **c**) in infected mice is associated with infiltration of macrophages (arrows in **d**), where $CD3^+$ (**e**) and IFN-γ^+ (arrows in **f**) lymphocytes are visible. Intense FAS^+ cholangiocytes (rectangles in **g**) with $FASL^+$ lymphocytes (arrows in **h**) and $FASL^+$ cholangiocytes (rectangle in **h**) are seen. 12 d postinjection. **c**, **d**, **f** (white star): bile ductal lumen; **a**–**d**, **f**: IF; **e**, **g**, **h**: IHC (positive cells: brown color, counterstained by Mayer's hematoxylin). **a**–**d**, **f**–**h**: original magnification ×750 and **e**: original magnification ×350. Bar = 50 μm. IF, immunofluorescence; IHC, immunohistochemistry.

degrees of expression of these antigens and cytokines in cholangiocytes and inflammatory cells at 12 dpi are summarized in **Table 1**.

Foxp3⁺ Cells in Bile Duct Lesions, Regional Lymph Nodes, and Thymi

The number of Foxp3⁺ cells in inflamed ductal lesions of the infected group (**Figures 5a**) was similar to that of the control group (**Figure 5b**). The number of Foxp3⁺ cells decreased in regional lymph nodes at 5 dpi, but not at 10 dpi, and in thymi at 10 dpi, but not at 5 dpi, in the infected group (**Figure 5c–l**).

Table 1. Degree of expression of antigens and cytokines (molecule) in and/or on cholangiocytes and mononuclear cells

Molecule	Cholangiocyte	Lymphocyte	Macrophage
MHC class I	+++	+	+
CD3	–	+++	–
IFN-γ	–	+++	–
CD4	–	+++	–
CD8	–	+++	–
FAS	+++	+	–
FASL	++	+	–
TNF-α	–	+++	+++

–, no; +, weak; ++, moderate; +++, intense; MHC, major histocompatibility complex.

DISCUSSION

In this study, we demonstrated Reo-2–mediated biliary destruction and proposed two different mechanisms that may explain Reo-2–induced epithelial destruction. First, viral replication occurs shortly after infection (initiation phase), leading to duct destruction. Second, an autoimmune-mediated process (effector phase) develops in the destruction of duct.

During the initiation phase, two types of duct destruction such as necrosis and apoptosis may be induced by Reo-2. Wilson *et al.* (10) demonstrated that the Reo-3 S1 gene is important for the determination of viral tropism in cholangiocytes. Attachment of reovirus to target cells is mediated through the filamentous, trimer reovirus sigma 1 protein, which is a serotype-independent receptor (15). Thus, the same mechanism may operate in Reo-2 infection, resulting in cell necrosis. Moreover, reovirus-induced apoptosis will be induced by the release of TNF-related apoptosis-inducing ligand (TRAIL) from infected cells and the activation of TRAIL-associated death receptors, death receptor 4 and death receptor 5, leading

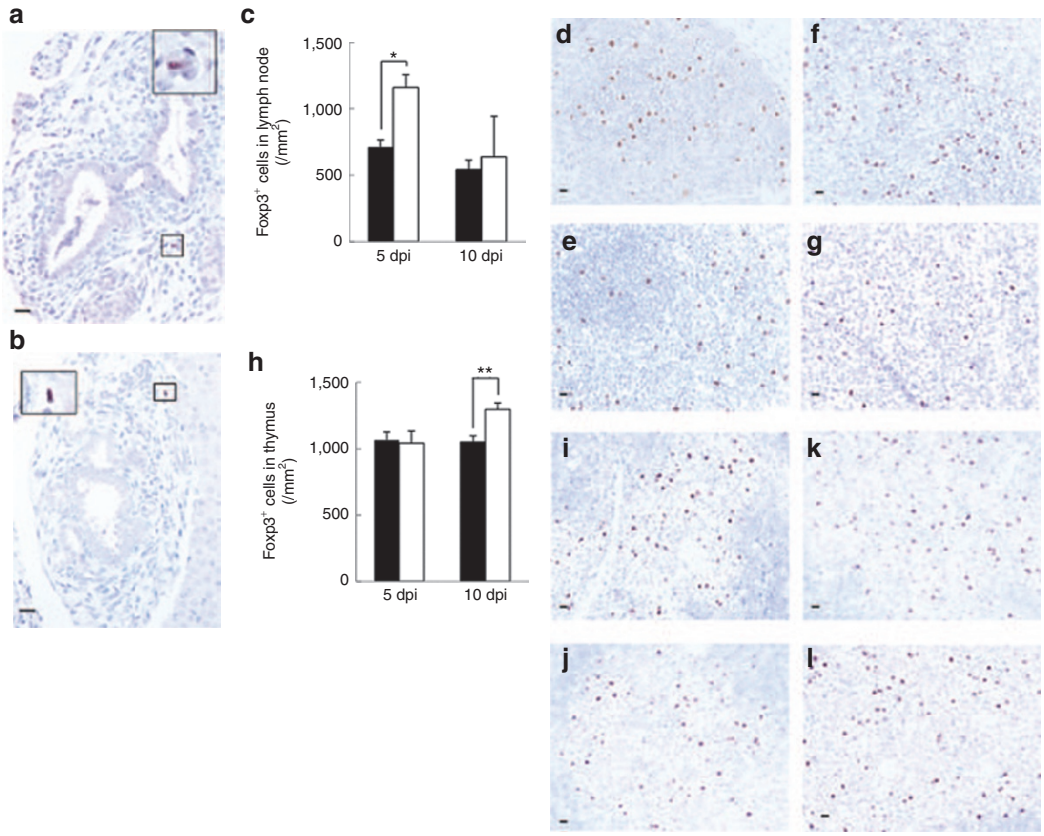

Figure 5. Foxp3⁺ cells in (**a**,**b**) bile ducts, (**c**,**d**,**e**,**f**,**g**) lymph nodes, and (**h**,**i**,**j**,**k**,**l**) thymi. (**a** and enlarged rectangle in **a**) No increase of Foxp3⁺ cells in bile ducts of the infected mice compared with (**b** and enlarged rectangle in **b**) the control mice. Numbers of Foxp3⁺ cells decreased in regional lymph nodes at 5 dpi, but not at 10 dpi, in (**c**,**d**,**e**) the infected mice compared with (**c**,**f**,**g**) the control. Decreased numbers of Foxp3⁺ cells in the infected mice at 10 dpi, but not at 5 dpi, in (**h**,**i**,**j**) thymi compared with (**h**,**k**,**l**) the control. **a**, **b**, **d**–**g**, **i**–**l**: IHC (Foxp3⁺ cells: brown color, counterstained by Mayer's hematoxylin). **d**,**e**,**i**,**j**: 5 dpi and **f**,**g**,**k**,**l**: 10 dpi. **a**, **b**: ×400; **d**–**g** and **i**–**l**: ×200; insets of **a** and **b**: ×600 (original magnification). Bar = 50 μm. **c** and **h** (black columns: Reo-2–infected mice and white columns: control mice), mean ± SEM. $^{*}P < 0.05$, $^{**}P < 0.01$. dpi, days postinfection; IHC, immunohistochemistry.

to apoptosis (16). It may operate in the present study, since apoptosis was observed.

The initial damage to cholangiocytes by Reo-2 may result in release of cholangiocyte-specific antigens, which facilitate immune responses during effector phase that ultimately exacerbate ductal damage. There are several possibilities supporting this idea as follows. There is specific autoantibodies production against the cytoplasm of cholangiocytes, suggesting that biliary duct destruction may be due to duct-specific immune-mediated mechanisms. Thus, induction of biliary pathology may occur still despite the absence of virus, underscoring a cholangiocyte antigen-mediated destruction pathway. The penetration of mononuclear cells into cholangiocytes (epitheliotropism) is considered a key process for autoimmune-mediated destruction of biliary epithelium, which is typically followed by apoptosis and necrosis of epithelia (17). $CD8^+$ T cells, which are responsible for apoptosis of the biliary epithelium (18), respond to robust increases to major histocompatibility complex–coupled epithelial antigens. In addition, $FASL^+$ T cells respond to overexpressed FAS in ductal cells, which are caused by IFN-γ signaling from Th1 cells (19), leading to the destruction of biliary epithelia (17). $FASL^+$ cholangiocytes suggest that FASL upregulation may result in apoptotic fratricide of cholangiocytes other than $FASL^+$ lymphocytes injury to FAS^+ epithelia (2). In addition, apoptosis of lymphocytes was often observed, which was likely associated with activated T-cell expression of FAS and FASL, because FASL is not normally expressed on cholangiocytes, but those cells of all biliary atresia patients expressed FASL (2).

Increase in systemic production of IFN-γ, including infiltration of IFN-γ^+ lymphocytes, suggests a Th1 response (17), which may result from a host response to cholangiocyte antigens. Moreover, higher IFN-γ mRNA expression from splenic cells was detected at effector phase than at viral multiplication phase in the same experimental protocol of our previous report (6). Notably, these findings were associated with IFN-γ production in infants with biliary atresia. Bezerra *et al.* (20) discussed the recent support of the working hypothesis that proinflammatory signaling of lymphocytes is an important effector of epithelial injury in biliary atresia. Moreover, Orth *et al.* (21) reported a marked increase in IFN-γ production in a cholangitis rat model and suggested that IFN-γ may facilitate secretion of proinflammatory cytokines by macrophages. Alternatively, a lack or a little of IL-4 production in Reo-2–infected mice may result from mutually antagonistic effects of IFN-γ (one of representative Th1 cytokines) (6). Moreover, production of reactive oxygen species from infiltrated macrophages may contribute to apoptosis and necrosis of cholangiocytes (22).

$Foxp3^+$ regulatory T cells (Tregs) produce immunosuppressive cytokines, such as TGF-β, IL-10, and IL-35 and maintain peripheral auto-tolerance (23,24). Decreased TGF-β production may be, at least in part, due to decreased number of Tregs. Lack of inducible Tregs in ductal lesions with less accumulation of inducible Tregs in lymph nodes and naturally occurring Tregs in thymi may permit the development of autoimmune cholangitis. Regarding naturally occurring Tregs in thymi, it has been recently shown that the transfer of *in vitro*–generated naturally occurring Tregs, but not *in vitro*–generated inducible Tregs, into Foxp3-deficient mice increases survival (25), suggesting that there may be functional differences between naturally occurring Tregs and inducible Tregs. Alternatively, dendritic cells were recognized in inflamed ducts. Dendritic cells, which are professional antigen-presenting cells that present antigen to naïve T cells, may also play a role in suppressing the function of Tregs(26,27). Further study is needed to clarify the interaction between Tregs and dendritic cells in the development of autoimmune cholangitis.

Obstruction of bile ducts by fibrosis developed in weanling mice, but the disease was subclinical, and most mice recovered within 3 wk after infection. This is different from the human infantile biliary atresia with progressive biliary ductal lesions. However, immune-mediated damage of bile ducts may provide insights to the biliary pathology associated with human infantile biliary atresia. It has been proposed that biliary atresia may be the result of "a multiple-hit phenomenon", which combines the actions of several insult factors (2). For example, macrophages release cytokines, especially TGF-β, that can stimulate hepatic stellate cells to synthesize and secrete collagen, resulting in the development of portal fibrosis and cirrhosis, which are detected in ductal lesions (28). In addition, it has been reported that bacterial components (e.g., intestinal lipopolysaccharides) may stimulate macrophages to produce enough TGF-β from those cells, resulting in induction of severe fibrosis (29). It seems likely, because biliary epithelial cells constantly express at least Toll-like receptors 2–5 and can respond to the Toll-like receptor ligands (lipopolysaccharides) derived from the duodenum (30). In addition, it has been pointed out that IL-17A promotes the development of several autoimmune diseases as one of the factors (31). However, production of IL-17A was not observed in infected mice. Taken together, these may be the reasons why infected mice did not harbor persistent biliary lesions.

Reo-2 infection also causes autoimmune insulitis with impaired glucose tolerance by targeting glutamic acid decarboxylase (unpublished data). One might expect that Reo-2–induced cholangitis may be non–organ-specific process. However, similar outcomes were reported in rotavirus-induced biliary atresia. In these cases, the appearance of diabetes-associated autoantibodies against glutamic acid decarboxylase and IA-2 indicated that β cells were targeted, instead of ductal cells (32).

In conclusion, Reo-2 infection in mice confers many similar outcomes to the human infections, with a notable exception that fibrotic lesions are less severe in mice. Further work is required to confirm that environmental factors contribute to progressive biliary atresia or whether the Reo-2 virus can trigger infantile biliary atresia in humans.

METHODS

Virus Isolation

The BN-77 Reo-2 strain, isolated from bovine diarrheal matter, was grown on HmLu-1 cells as described previously (33). One-day-old mice were i.p. infected with 5×10^5 plaque-forming units per 0.05 ml with Dulbecco's modified Eagle's medium (DMEM; Nissui, Tokyo, Japan) (designated as day 0).

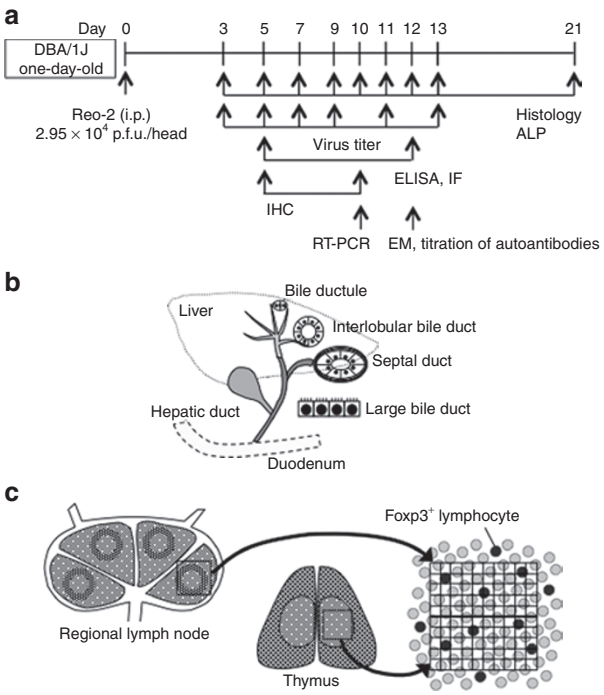

Figure 6. (**a**) Experimental protocol, (**b**) scheme of counting bile duct cells, and (**c**) Foxp3$^+$ cells. See Methods for details. ALP, alkaline phosphatase; EM, electron microscope; IF, immunofluorescence; IHC, immunohistochemistry; i.p., intraperitoneal; p.f.u., plaque-forming unit; RT-PCR, real-time PCR.

Infection of Mice

One-day-old DBA/1J mice of both sexes (Seac Yoshitomi, Fukuoka, Japan) were divided into Reo-2–infected and age-matched uninfected control groups. Mice were sacrificed as in **Figure 6a** (infected group: $n = 5$ and control group: $n = 4$ at each time point unless otherwise stated). They were kept at 24 ± 2°C in dry-heat–sterilized metal cages. Mother mice were fed with autoclaved commercial pellet (CE-2; CLEA, Tokyo, Japan) and were freely supplied sterilized water. The Animal Research Ethics Board of the Faculty of Agriculture at Yamaguchi University approved the animal experiments.

Virus Titration in Liver

Whole blood was obtained while exogenous viral contamination was carefully avoided. Subsequently, 20 mg of liver was resected from the left side of 5 Reo-2–infected mice and pooled (100 mg total). Liver samples were then homogenized in 1 ml of DMEM and centrifuged at 3,000*g* for 10 min. The titers, performed in duplicate, were determined by inoculating a monolayer of HmLu-1 cells in 35-mm dishes (Sumitomo, Tokyo, Japan) with 0.2 ml of 10-fold diluted supernatants. After adsorption for 2 h at 37°C, the monolayers were overlaid with DMEM-20% fetal calf serum and 0.8% agar, incubated at 37°C for 6 d and overlayed with DMEM-20% fetal calf serum, 0.8% agar, and 1% neutral red. Plaques were counted, and the viral titers (plaque-forming units per milliliter) were presented in $\log_{10}$ units.

Alkaline Phosphatase Value in Serum

Serum alkaline phosphatase concentrations were measured to assess the degree of biliary injury. Alkaline phosphatase values were determined using Fuji Dry-chem 5500s (Fuji Film, Tokyo, Japan) and expressed as IU/l.

Histopathology of Bile Duct Epithelium

Bile ducts were examined based on the anatomical location illustrated by Nakanuma *et al.* (17). Liver tissues were fixed in 10% neutral buffered formalin, embedded in paraffin, sectioned at 6 μm, and stained with hematoxylin and eosin and Masson's trichrome. Histopathological examination and grading were performed as described previously (21) with simple modifications. In brief, epithelial cell damage, infiltration (inflammation) of the bile duct, epithelium proliferation, and fibrosis were graded as follows: 0 = none, 1 = minimal, 2 = mild, 3 = moderate, 4 = severe. Score Index of each bile duct is calculated as $[(n_0 \times 0) + (n_1 \times 1) + (n_2 \times 2) + (n_3 \times 3) + (n_4 \times 4)]/\Sigma n$. Score Index and SD were calculated from four different parts of extrahepatic bile ducts randomly and blindly selected from each liver section by two investigators.

Detection of Viral Antigens in Biliary Epithelia

Paraffin sections of Reo-2–infected mice at 5 and 12 dpi ($n = 3$ for each time point) were probed with rabbit anti-Reo-2 antibody, followed by incubation with fluorescein isothiocyanate (FITC)–labeled goat antirabbit secondary antibody (Leinco, Manchester, UK). Uninfected mice were used as controls ($n = 2$).

Titration of Autoantibodies Against Cholangiocytes and Nuclei

Autoantibodies against cholangiocytes and nuclei in sera at 12 dpi (infected: $n = 13$ and control: $n = 5$) were assayed by indirect immunofluorescence (IF). Frozen sections of liver and pancreas from a healthy adult female DBA/1J mouse were blocked with goat serum and then incubated with goat FITC-labeled antimouse IgG/M/A (Serotec, Oxford, UK). The IF titers were expressed as the reciprocal of the lowest dilutions that had a positive response and were transformed to $\log_2$ scale. To confirm the specificity of the reaction, IF-positive sera were subjected to absorption test with liver extract from normal weanling DBA/1J mouse. The titer from sera of infected mice over $\log_2$ 4 that of control mice was considered as the lower limit of positive value.

IF and Immunohistochemistry

For IF, the liver samples at 12 dpi (infected: $n = 3$ and control: $n = 2$) were frozen in chilled *n*-hexane, sectioned at 4 μm by cryostat, and fixed in acetone. Sections were treated with primary antibodies as follows: rat antimouse major histocompatibility complex class I monoclonal antibody (mAb) (clone: ERMP42; Abcam Japan, Tokyo, Japan), FITC-conjugated rat antimouse IFN-γ mAb (clone: 05-142; Upstate Biotechnology, Lake Placid, NY), FITC-conjugated rat antimouse CD4 (L3/T4) mAb (clone: YTS 191.1; Cedarlane, Westbury, NY), FITC-conjugated rat antimouse CD8 mAb (clone: SE-A1006; Sumitomo Electric, Osaka, Japan), and FITC-conjugated rat antimouse macrophage (clone: MCA519; Serotec). The sections that reacted with anti–major histocompatibility complex class I antibody were incubated with FITC-conjugated goat antirat immunoglobulin secondary antibody (Biosource, Camarillo, CA).

The paraffin sections of the livers, regional (hepatic) lymph nodes, and thymi at 5 or 10 dpi were autoclaved in Dako Target Retrieval Solution (pH 6; Dako Japan, Tokyo, Japan) at 120°C for 5 min or Dako Target Retrieval Solution (pH 9) at 121°C for 1 min. Endogenous peroxidase activity was inactivated with 3% aqueous hydrogen peroxide for 10 min. Then, sections were treated with Protein Block Serum-Free (Dako Japan) for 30 min to block nonspecific binding of antibodies. Sections were treated with primary antibodies overnight as follows: rabbit antihuman CD3 polyclonal antibody (Dako Japan), rat antimouse Foxp3 mAb (clone: NRRF-30; eBioscience, San Diego, CA), rabbit antimouse FAS polyclonal antibody (Santa Cruz Biotechnology, Santa Cruz, CA), rabbit antihuman FASL polyclonal antibody (Abcam Japan), and rabbit antimouse TNF-α polyclonal antibody (Abcam Japan). Thereafter, sections were incubated with the Histofine Simple Stain MAX-PO (R) or (Rat) (Nichirei Bioscience, Tokyo, Japan). Positive reactions were visualized with 3′3-diaminobenzidine tetrahydrochloride (Roch Diagnostic, Penzberg, Germany), and sections were counterstained with Mayer's hematoxylin.

All incubations were done at room temperature except for those of primary antibodies (4°C). To test the specificity, the reaction without the primary antibody served as a negative control.

Electron Microscopy

At 12 dpi, a part of the liver (infected: $n = 3$ and control: $n = 2$) was fixed in 1% osmium tetroxide and embedded in Epon 812. The orientation of the blocks was achieved by examining 1-μm sections stained with toluidine blue. Ultrathin sections were stained with

uranyl acetate and lead nitrate and observed by electron microscopy (H-7600; Hitachi, Ibaraki, Japan) at 80 kV.

Detection of Apoptosis of Cholangiocyte and Infiltrated Lymphocyte by TUNEL Staining

DNA fragmentation of apoptotic cells at 5 and 12 dpi was visualized by enzymatic reaction in paraffin sections (n = 3 in each group at each time point) using the *in situ* cell detection kit (Enzo, Penzberg, Germany). In brief, deparaffinized sections were incubated in 20 μg/ml of proteinase K to strip proteins from nuclei and then in 0.3% H_2O_2 methanol to abolish endogenous peroxidase activity. Subsequently, TdT buffer solution containing TdT and fluorescein-labeled dUTP was added. The sections were reacted with peroxidase-conjugated antifluorescein antibody. The reaction products were visualized by a benzidine reaction, and sections were counterstained with Mayer's hematoxylin.

ELISA for Serum Levels of IFN-γ, IL-4, IL-17A, and TGF-β1

The concentrations of IFN-γ, IL-4, IL-17A, and TGF-β1 at 5 and 12 dpi were measured with ELISA kit for mouse IFN-γ (Genzyme Techne, Minneapolis, MN), IL-4 (American Research Products, Cambridge, MA), IL-17A (eBioscience), and TGF-β1 (Genzyme Techne). Detectable amounts of IFN-γ, IL-4, IL-17A, and TGF-β1 are 2.0, 1.6, 4, and 1.6 pg/ml, respectively. In cases where cytokines were not detected, their concentration was assigned a value of 0 pg/ml.

Detection of mRNA Expression of IL-4, IFN-γ, and IL-17A in Spleen

Total RNA was isolated from frozen spleen samples (n = 3 in each group) at 10 dpi with TRI reagent (Molecular Research Center, Cincinnati, OH). One microgram of total RNA was treated with Turbo DNA-free (Applied Biosystems, Tokyo, Japan) and transcribed into cDNA using Superscript III (Invitrogen, Tokyo, Japan). Oligo dT primers were used to prime the first-strand synthesis for each reaction. After single-strand cDNA was generated, it was subjected to real-time PCR amplification with a QuantiTect SYBR Green PCR Kit (Qiagen, Valencia, CA). The primers used for amplification of IFN-γ (33), IL-4 (34), IL-17A (35), and glyceraldehyde-3-phosphate dehydrogenase (GAPDH) (36) are as follows:

IFN-γ: forward, 5′-TCAAGTGGCATAGATGTGGAAGAA-3′ and reverse, 5′-TGGCTCTGCAGGATTTTCATG-3′; IL-4: forward, 5′-ACAGGAGAAGGGACGCCAT-3′ and reverse, 5′-GAAGCCCTACAGACGAGCTCA-3′; IL-17A: forward, 5′-TCCAGAAGGCCCTCAGACTA-3′ and reverse, 5′-AGCATCTTCTCGACCCTGAA-3′; and GAPDH: forward, 5′-TCACCACCATGGAGAAGGC-3′ and reverse, 5′-GCTAAGCAGTTGGTGGTGCA-3′.

Each assay was performed in duplicate. Predenaturation at 95°C for 15 min was followed by 45 cycles of PCR amplification consisting of denaturation at 94°C for 15 s, annealing at 60°C for 30 s, and extension at 72°C for 30 s. PCR and fluorescence intensity detection were performed with the StepOne PCR system (PerkinElmer, Waltham, MA). The data were analyzed using StepOne software v.2.0. Briefly, the PCR cycle number at the threshold was represented as C_T. The difference between C_T values for the target and internal control, i.e., ΔC_T, was calculated. The value of $2\Delta C_T$ was considered representative of the amount of target mRNA relative to the amount of internal control.

Measurement of Tregs in Ducts, Regional Lymph Nodes, and Thymi

The number of Foxp3$^+$ cells in hepatic lymph nodes (lymphoid nodules) and thymi at 5 and 10 dpi (n = 3 in each group at each time point) was counted using an eyepiece micrometer. This method was favored over fluorescence-activated cell sorter analysis of peripheral blood leukocytes because it is very difficult to get adequate amounts of blood from weanling mice. Results were averaged from each group and represented as mean ± SEM.

Statistical Analysis

The means ± SEM or ± SD were calculated and analyzed by F-test and then by Student's t-test (one-tailed or two-tailed). The accepted level of significance was $P < 0.05$.

Disclosure: The authors declare no conflict of interest.

REFERENCES

1. Mack CL. The pathogenesis of biliary atresia: evidence for a virus-induced autoimmune disease. Semin Liver Dis 2007;27:233–42.
2. Sokol RJ, Mack C. Etiopathogenesis of biliary atresia. Semin Liver Dis 2001;21:517–24.
3. Bezerra JA. Biliary atresia–translational research on key molecular processes regulating biliary injury and obstruction. Chang Gung Med J 2006;29:222–30.
4. Shivakumar P, Campbell KM, Sabla GE, et al. Obstruction of extrahepatic bile ducts by lymphocytes is regulated by IFN-gamma in experimental biliary atresia. J Clin Invest 2004;114:322–9.
5. Tyler KL. Mammalian reoviruses. In: Knipe DM, Howley PM, Griffin DE, et al, eds. Fields Virology, 4th edn. Philadelphia, PA: Lippincott-William & Wilkins, 2001:1729–45.
6. Onodera T, Hayashi T. In: Taylor K, Hyöty H, Toniolo A, Zuckerman AA, eds. Reovirus in Diabetes and Viruses. New York, NY: Springer Science, 2013:71–80.
7. Clarke P, Richardson-Burns SM, DeBiasi RL, Tyler KL. Mechanisms of apoptosis during reovirus infection. Curr Top Microbiol Immunol 2005;289:1–24.
8. Papadimitriou JM. The biliary tract in acute murine reovirus 3 infection. Light and electron microscopic study. Am J Pathol 1968;52:595–611.
9. Bangaru B, Morecki R, Glaser JH, Gartner LM, Horwitz MS. Comparative studies of biliary atresia in the human newborn and reovirus-induced cholangitis in weanling mice. Lab Invest 1980;43:456–62.
10. Wilson GA, Morrison LA, Fields BN. Association of the reovirus S1 gene with serotype 3-induced biliary atresia in mice. J Virol 1994;68:6458–65.
11. Rosenberg DP, Morecki R, Lollini LO, Glaser J, Cornelius CE. Extrahepatic biliary atresia in a rhesus monkey (Macaca mulatta). Hepatology 1983;3:577–80.
12. Morecki R, Glaser JH, Johnson AB, Kress Y. Detection of reovirus type 3 in the porta hepatis of an infant with extrahepatic biliary atresia: ultrastructural and immunocytochemical study. Hepatology 1984;4:1137–42.
13. Tyler KL, Sokol RJ, Oberhaus SM, et al. Detection of reovirus RNA in hepatobiliary tissues from patients with extrahepatic biliary atresia and choledochal cysts. Hepatology 1998;27:1475–82.
14. Holmdahl R, Andersson M, Goldschmidt TJ, Gustafsson K, Jansson L, Mo JA. Type II collagen autoimmunity in animals and provocations leading to arthritis. Immunol Rev 1990;118:193–232.
15. Guglielmi KM, Johnson EM, Stehle T, Dermody TS. Attachment and cell entry of mammalian orthoreovirus. Curr Top Microbiol Immunol 2006;309:1–38.
16. Clarke P, Tyler KL. Reovirus-induced apoptosis: a minireview. Apoptosis 2003;8:141–50.
17. Nakanuma Y, Tsuneyama K, Harada K. Pathology and pathogenesis of intrahepatic bile duct loss. J Hepatobiliary Pancreat Surg 2001;8:303–15.
18. Shivakumar P, Sabla G, Mohanty S, et al. Effector role of neonatal hepatic CD8+ lymphocytes in epithelial injury and autoimmunity in experimental biliary atresia. Gastroenterology 2007;133:268–77.
19. Mack CL, Tucker RM, Sokol RJ, Kotzin BL. Armed CD4+ Th1 effector cells and activated macrophages participate in bile duct injury in murine biliary atresia. Clin Immunol 2005;115:200–9.
20. Bezerra JA, Tiao G, Ryckman FC, et al. Genetic induction of proinflammatory immunity in children with biliary atresia. Lancet 2002;360:1653–9.
21. Orth T, Neurath M, Schirmacher P, Galle PR, Mayet WJ. A novel rat model of chronic fibrosing cholangitis induced by local administration of a hapten reagent into the dilated bile duct is associated with increased TNF-alpha production and autoantibodies. J Hepatol 2000;33:862–72.
22. Laskin DL, Pendino KJ. Macrophages and inflammatory mediators in tissue injury. Annu Rev Pharmacol Toxicol 1995;35:655–77.
23. Sakaguchi S, Toda M, Asano M, Itoh M, Morse SS, Sakaguchi N. T cell-mediated maintenance of natural self-tolerance: its breakdown as a possible cause of various autoimmune diseases. J Autoimmun 1996;9:211–20.
24. Gravano DM, Vignali DA. The battle against immunopathology: infectious tolerance mediated by regulatory T cells. Cell Mol Life Sci 2012;69:1997–2008.

25. Haribhai D, Williams JB, Jia S, et al. A requisite role for induced regulatory T cells in tolerance based on expanding antigen receptor diversity. Immunity 2011;35:109–22.
26. Cronin SJ, Penninger JM. From T-cell activation signals to signaling control of anti-cancer immunity. Immunol Rev 2007;220:151–68.
27. Yamazaki S, Iyoda T, Tarbell K, et al. Direct expansion of functional CD25+ CD4+ regulatory T cells by antigen-processing dendritic cells. J Exp Med 2003;198:235–47.
28. Kisseleva T, Brenner DA. Role of hepatic stellate cells in fibrogenesis and the reversal of fibrosis. J Gastroenterol Hepatol 2007;22:Suppl 1:S73–8.
29. Bowen T, Jenkins RH, Fraser DJ. MicroRNAs, transforming growth factor beta-1, and tissue fibrosis. J Pathol 2013;229:274–85.
30. Harada K, Ohira S, Isse K, et al. Lipopolysaccharide activates nuclear factor-kappaB through toll-like receptors and related molecules in cultured biliary epithelial cells. Lab Invest 2003;83:1657–67.
31. Stockinger B, Veldhoen M. Differentiation and function of Th17 T cells. Curr Opin Immunol 2007;19:281–6.
32. Honeyman MC, Coulson BS, Stone NL, et al. Association between rotavirus infection and pancreatic islet autoimmunity in children at risk of developing type 1 diabetes. Diabetes 2000;49:1319–24.
33. Menon K, Wu Y, Haas J, Sahu SK, Yang B, Zaheer A. Diminished degradation of myelin basic protein by anti-sulfatide antibody and interferon-gamma in myelin from glia maturation factor-deficient mice. Neurosci Res 2007;58:156–63.
34. Miyake T, Inaba M, Fukui J, et al. Prevention of graft-versus-host disease by intrabone marrow injection of donor T cells: involvement of bone marrow stromal cells. Clin Exp Immunol 2008;152:153–62.
35. Hattori K, Nishikawa M, Watcharanurak K, et al. Sustained exogenous expression of therapeutic levels of IFN-gamma ameliorates atopic dermatitis in NC/Nga mice via Th1 polarization. J Immunol 2010;184:2729–35.
36. Peter M, Bode K, Lipford GB, Eberle F, Heeg K, Dalpke AH. Characterization of suppressive oligodeoxynucleotides that inhibit Toll-like receptor-9-mediated activation of innate immunity. Immunology 2008;123:118–28.